H_∞ Control for a Smart Micro-Positioning System with an Analytical Model for the Output of the Inverse Compensation

Micky Rakotondrabe, Omar Aljanaideh, and Mohammad Al Janaideh

***Abstract*— An experimental study was carried out on a piezoelectric actuator in order to explore the benefits of a mathematical formula [1], that describes the output of the inverse compensation when an inverse Prandtl-Ishlinskii hysteresis model is applied as a feedforward compensator. The inverse Prandtl-Ishlinskii was first formulated and applied for compensation of hysteresis nonlinearities of a piezoelectric actuator. The theoretical formula was afterwards employed to construct an H_∞ feedback control. The controller was calculated and applied to the piezoelectric actuator with the inverse feedforward model. The experimental results verify the effectiveness of the controller and the benefits that the theoretical formula of the inverse compensation can contribute.**

I. Introduction

In order to enhance the tracking performance of systems with hysteresis, considerable efforts have been made towards the design of control methods for compensation of the hysteresis effects [1]-[4]. Compensation hysteresis nonlinearities of smart material based actuators has been widely performed using Prandtl-Ishlinskii model due its suitability for real-time system applications [2]. The reported studies on hysteresis compensation using the inverse of Prandtl-Ishlinskii model however exhibit notable compensation errors. The hysteresis characterization errors can be considered as one of the main sources of the compensation errors when the inverse Prandtl-Ishlinskii model is employed to serve as a feedforward compensator [1]. Several micro-and nano-positioning systems employ the smart material-based actuators with a plant (dynamic system) in closed-loop control systems that consist of an inverse hysteresis model and a feedback control method to reduce the tracking errors between the reference input and the output of the plant. The output of the inverse compensation, which represents the output of the smart-material based actuator in the presence of the inverse hysteresis model, is considered as an input signal to the plant. Since measuring this signal is a challenging task, deriving a mathematical formula is essential to characterize the output of the inverse compensation.

In this paper, the output of the inverse compensation is characterized and employed in conjunction with an H_∞ controller to enhance the tracking performance of smart micro-and nano-positioning actuators. Consider Fig. 1 where the actuator system is typified by hysteresis that can be described using Prandtl-Ishlinskii model and a compensator that represents another Prandtl-Ishlinskii model implemented for cancellation the hysteresis of the model. y is called output of the inverse compensation (output of the system with feedforward controller), u is the command (driving) input and v is the reference input of the feedforward scheme (input of the compensator). In general, the actuator is integrated in a more complex plant with lower dynamics where the plant output x is measurable and the actuator output y is non-measurable.

This paper represents a theoretical formulation for the non-measured output y versus the input v when the Prandtl-Ishlinskii hysteresis model is not exact or incorporates uncertainty. Such formula can be used in a structural analysis (stability), performance analysis, or in synthesizing a feedback controller such that the overall feedforward-feedback control scheme ensures some stability/performance in presence of the model uncertainty.

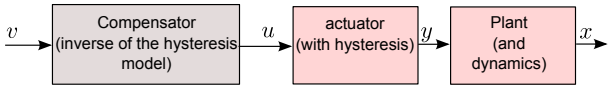

Fig. 1. Block diagram of a feedforward controlled system with hysteresis.

The derivation of the formula $y\left(v(t),t\right)$, of the compensated output y versus the input v when the Prandtl-Ishlinskii hysteresis model is not exact has been described in [1]. This formula is employed in this paper to construct an H_∞ feedback controller for a piezoelectric actuator.

II. Background

In this section the theoretical results obtained in [1] are revisited.

A. The output of the inverse compensation

For a given input $v(t) \in C[0,T]$, the output of the inverse compensation when the estimated inverse $\hat{\mathcal{P}}^{-1}$ is employed as a feedforward compensator for compensation of hysteresis nonlinearities defined by the Prandtl-Ishlinskii model $\mathcal{P}$ can be described as

$$\mathcal{P} \circ \hat{\mathcal{P}}^{-1}[v](t) = p_{0\eta} v(t) + \int_0^R p_\eta(r) \mathcal{F}_r[v](t) dr, \qquad (1)$$

where $\mathcal{F}_r[v](t)$ is the output of the play operator, $p_{0\eta}$ is a positive constant, and $p_\eta(r)$ is the density function.

M. Rakotondrabe is with the Department of Automatic Control and Micro-Mechatronic Systems depart. (AS2M), FEMTO-ST Institute, CNRS - University of Franche-Comt at Besanon (UFC) - ENSMM - UTBM, Besanon France, email: mrakoton@femto-st.fr.

O. Aljanaideh is with the Department of Mechanical Engineering, The University of Jordan, Amman 11942, Jordan. email: omaryanni@gmail.com

M. Al Janaideh is with the Department of Mechatronics Engineering, The University of Jordan, Amman 11942, Jordan. email: aljanaideh@gmail.com

B. Boundedness

The first term in (1) describes a linear reversible term, while the second is assumed to be bounded. Analytically

$$\mathcal{P} \circ \hat{\mathcal{P}}^{-1}[v](t) = \rho v(t) + \Omega(t), \tag{2}$$

where ρ is a positive constant $\rho = p_{0\eta} + \int_0^R p_\eta(r)dr$, $\Omega(t)$ is a nonlinear term bounded by a positive constant, $|\Omega(t)| \leq \xi$, where [1]

$$\xi \leq |\int_0^R r p_\eta(r)dr|. \tag{3}$$

III. Experimental case: application to a piezoelectric actuator (PEA)

A. Presentation of the setup

A piezoelectric actuator of a cantilevered structure (piezo-cantilevered) has been acquired for the experimental study. The high resolution, high bandwidth and the high stiffness make these actuator well-suited for micromanipulation and microassembly of small objects [8], actuation in micromirror orientation and miniaturized bio-inspired robots [9] [11], scanning in atomic force microscopy (AFM) [10].

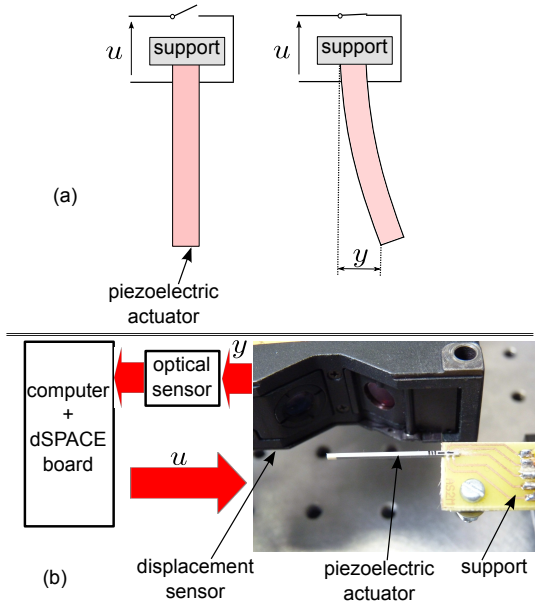

Fig. 2. (a) a piezoelectric cantilevered actuator, and (b) schematic representation of the setup.

In this paper, a PEA is constructed with several layers (multilayer), that allows obtaining a high range of bending at low voltages. When an input voltage $u(t)$ is applied to all the layers, a bending $y(t)$ is contributed at the tip of the actuator (Fig. 2-a). The experimental setup is presented in Fig. 2-b and includes:

- a multilayered piezoelectric cantilevered actuator (with 36 layers) of dimensions (active length $\times$ width $\times$ thickness) of: $15mm \times 2mm \times 2mm$,
- an optical displacement sensor has been acquired for measurement of actuator displacement. The sensor (LC2420 from Keyence) has a $10nm$ resolution, $100nm$ precision and more than $1kHz$ bandwidth,
- a computer with Matlab-Simulink software to synthesis input signals and to formulate the (feedforward and feedback) controllers,
- and a dSpace board that serves as DAC/ADC converter between the computer and the other parts of the experimental setup.

B. Characterization

A sinusoidal input voltage u was applied to the PEA at sufficient excitation frequency ($f = 0.1Hz$) that avoids both the phase-lag and creep effects [2]. Fig. 3 pictures experimental results attained at amplitude of $5V$ and $10V$ which is the maximal operating range of the actuator. The hysteresis amplitude of the PEA was found as 16.3% ($= \frac{h_{hyst}}{H_{hyst}} \approx \frac{14\mu m}{86\mu m}$).

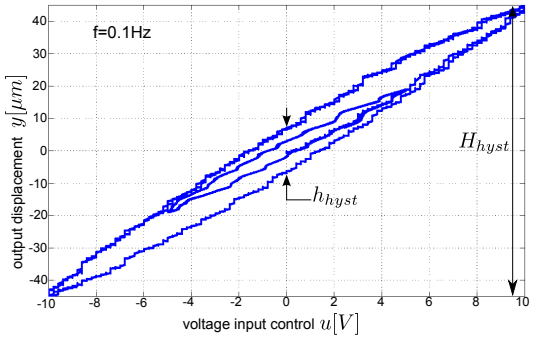

Fig. 3. Hysteresis obtained from the PEA under a sinusoidal driving voltage $u(t) = 10\sin(2\pi 0.1t)$.

C. Modeling and parameters identification of the hysteresis and dynamics of the actuator

The measured major hysteresis loop (obtained at $10V$ amplitude) was considered with its own initial loading curve for identification of the model parameters. 15 play operators were employed in the identification procedure which is described in details in [2]. The identified thresholds and weights of the model were found as

$$\begin{cases} r_i = \{0.095, 0.38, 0.84, 1.46, 2.21, 3.07, 4.01 \\ \quad 4.98, 5.96, 6.89, 7.76, 8.52, 9.14, 9.61, 9.9\} \\ p_i = \{2.55, 0.57, 1.3, -1.57, 1.25, -0.054, -0.032, 0.66 \\ \quad 0.16, -0.77, 2.02, -1.63, -0.15, 2.99, -1.09\} \end{cases} \tag{4}$$

The hysteresis curve of the model using the parameters (4) was obtained and compared to the measured response of the actuator in the presence of the initial loading curve in Fig. 4. The comparison revealed a good agreement between the model response and measured data. The dynamics of the actuator was afterwards identified by applying a step input $u = 10V$ to the PEA. The step response of the actuator is pictured in Fig. 5 (solid line), which shows an oscillation at nearly $400Hz$ frequency. The ARMAX (Auto Regressive Moving Average with external inputs) parametric identification technique [12] was considered to identify the dynamics of the actuator $D(s)$ which was normalized afterwards to obtain $D(s = 0) = 1$ and found as

$$D(s) = \frac{-20.7\big(s-1.22\times10^5\big)\big(s+2.99\times10^4\big)\big(s-2.776\times10^4\big)}{(s^2+925s+4.59\times10^5)(s^2+55s+1.4\times10^7)} \\ \frac{\big(s-1.07\times10^4\big)(s+1430)\big(s^2+4.3\times10^4 s+3.2\times10^9\big)}{(s^2+1.54\times10^4 s+4\times10^9)(s^2+964s+3.95\times10^9)}. \quad (5)$$

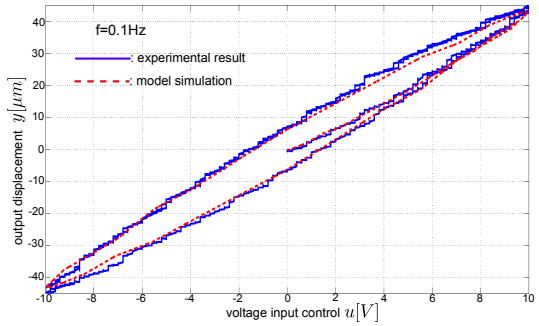

Fig. 4. Hysteresis of the PEA at $0.1Hz$: comparison of the experimental result with the model simulation.

A comparison between the step response of the actuator and the identified dynamics is displayed in Fig. 5, as the figure illustrates the function $D(s)$ can describe the dynamics of the actuator.

D. Hysteresis compensation using the inverse Prandtl-Ishlinskii model

The compensation of the hysteresis nonlinearities of the actuator was carried out using the inverse Prandtl-Ishlinskii model. The scheme of the compensation is presented in Fig. 6 where v is the input, u is the driving voltage and y is the output displacement which is also called the output of the inverse compensation. In this figure, the measured hysteresis of PEA actuator (Fig. 3) is denoted as $\mathcal{P}$, was characterized using the Prandtl-Ishlinskii model $\hat{\mathcal{P}}$ which is an approximation of the measured data. The parameters of the model (4) were employed to formulate the compensator $\hat{\mathcal{P}}^{-1}$ which is also a Prandtl-Ishlinskii model, that has the following thresholds and weights:

$$\begin{cases} z_i = \{0, 0.72, 2.16, 4.89, 7.04, 10.58, 14.36, 18.26, 22.81 \\ 27.34, 30.85, 35.46, 38.24, 40.24, 42.35\} \\ g_i = \{0.39, -0.072, -0.094, 0.12, -0.11, 0.0033, 0.002 \\ -0.035, -0.007, 0.04, -0.082, 0.06, 0.008, -0.095, 0.024\} \end{cases} \quad (6)$$

The compensator $\hat{\mathcal{P}}^{-1}$ was synthesized in the MATLAB/Simulink environment and applied via dSpace ControlDesk software to the PEA following to obtain the identity $y = v$ as the scheme in Fig. 6 illustrates. The output of the PEA with the inverse compensator is displayed in Fig. 7 which shows the experimental result of the output of the inverse compensation $y = \mathcal{P} \circ \hat{\mathcal{P}}^{-1}[v]$ versus the input v. The results demonstrate that the hysteresis cannot vanish when the inverse Prandtl-Ishlinskii model $\hat{\mathcal{P}}^{-1}$ is applied as a feedforward compensator. The remaining error after compensation can be expressed as $\epsilon = v - \mathcal{P} \circ \hat{\mathcal{P}}^{-1}[v]$, which is attributed to the fact that the identified model $\hat{\mathcal{P}}[u]$ is an approximation of the real hysteresis $\mathcal{P}$. The error, as Fig. 7 illustrates, has an amplitude of 3.75% $(= \frac{h_{hyst}}{H_{hyst}} \approx \frac{3\mu m}{80\mu m})$. This error as described in (2) has a linear reversible term and a nonlinear bounded term, this observations will be employed to design a feedback controller for the compensated output of the PEA.

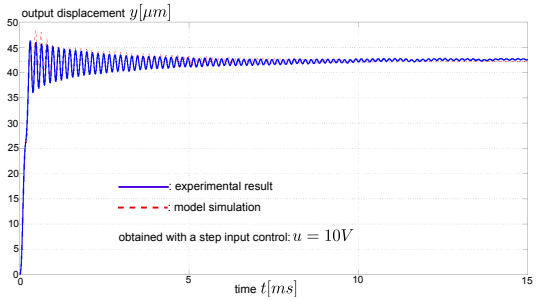

Fig. 5. Step response of the PEA with $u = 10V$: comparison of the experimental result with the model simulation.

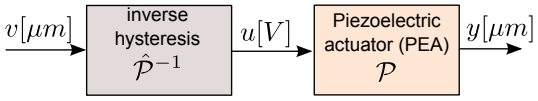

Fig. 6. Compensation of hysteresis using the cascade arrangement of the model $\hat{\mathcal{P}}$ and its inverse $\hat{\mathcal{P}}^{-1}$.

E. H_∞ control of the piezoelectric actuator with inverse compensation

Synthesizing a feedback controller for the inverse compensated PEA pictured in Fig. 7 is presented in this section. The identified normalized dynamics $D(s)$ in (5) was incorporated for designing the controller. The system to be controlled has therefore the input $v[\mu m]$ and the output $x[\mu m]$ as illustrated in Fig. 8-a.

1) Model for the feedback control synthesis: As described in (1), the inverse compensation $\mathcal{P}o\hat{\mathcal{P}}^{-1}[v]$ can be expressed by a linear operator ρ followed by a bounded nonlinear term Ω, that is:

$$\begin{aligned} & y(t) = \mathcal{P}o\hat{\mathcal{P}}^{-1}[v(t)] = \rho v(t) + \Omega[v(t), t] \\ & \Leftrightarrow \\ & y(s) = \mathcal{P}o\hat{\mathcal{P}}^{-1}[v(s)] = \rho v(s) + \Omega[v(s), s]. \end{aligned} \quad (7)$$

Including the dynamics $D(s)$ in (7) yields

$$\begin{aligned} & x(s) = D(s)y(s) = D(s)\mathcal{P}o\hat{\mathcal{P}}^{-1}[v(s)] \\ & = D(s)\left(\rho v(s) + \Omega[v(s), s]\right) \\ & \Leftrightarrow \\ & x = \rho D(s)v + \Omega_x, \end{aligned} \quad (8)$$

where $\Omega_x = D(s)\Omega$ is the output disturbance. Accordingly, the equivalent block diagram with the simplified notation $G(s) = \rho D(s)$ that represents the linear system to be controlled is illustrated in Fig. 8-b . Our aim is to find a (linear) controller $C(s)$ that permits the system $G(s)$ to track the reference and desired input x_d, and rejects the

external disturbance Ω_x (see Fig. 9-a). The tracking error in the figure e can be expressed as $e = x_d - x$. The standard H_∞ technique is considered an efficient way to achieve the tracking specifications and the disturbance rejection during the controller synthesis.

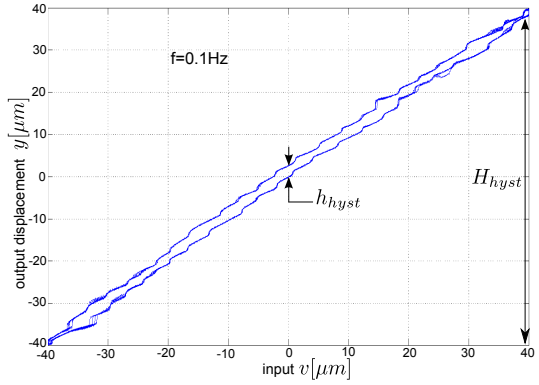

Fig. 7. Experimental result of the output inverse compensation.

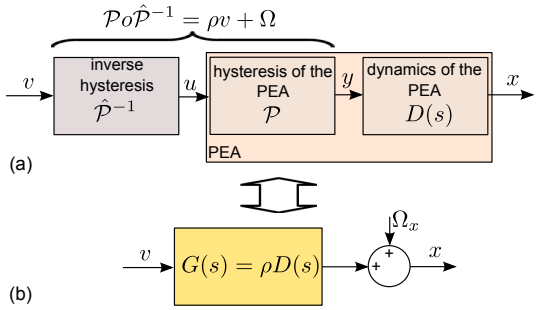

Fig. 8. The system to be controlled by a feedback controller.

Notice that the static gain ρ was identified as the identity mapping of (v, y) relationship in Fig. 6 which results $\rho = \frac{40\mu m}{40\mu m} = 1$. From the same figure, the term Ω can be also characterized. In fact, this term contributes the residual hysteresis to the ρv term. An appropriate characteristic of Ω could be observed when $\frac{h_{hyst}}{H_{hyst}}$ is maximal. This worst case was explored at the maximum operating range which was found less than $3\mu m$ as Fig. 7 illustrates. Consequently, for $y = 1v + \Omega$, the bound $|\Omega| < 3\mu m$ will be considered as the worst case characteristic. Since the dynamics $D(s)$ is normalized, the output disturbance $\Omega_x = D(s)\Omega$ has a bound of $3\mu m \times (1 + \delta_D)$, where δ_D is the overshoot which can be calculated from Fig. 5 as $\delta_D = 9.5\%$. Accordingly, $\Omega_x^{max} = 3.285\mu m$ will be considered in the controller synthesis as the worst case of Ω_x . $\Omega_x^{max} = 3.285\mu m$.

2) Specifications: The specifications employed to calculate the H_∞ controller $C(s)$ are as the following.

a) Tracking performance:

- the initial overshoot of 9.5% should be completely damped for the closed-loop,
- the statical tracking error should be less or equal to 0.1%,
- and the settling time should be less or equal to $3ms$.

b) Disturbance rejection: The disturbance effect Ω_x^{max} have to be negligible at the output. An $\Omega_x^{max} = 3.285\mu m$ was selected which yields a maximal error of $e^{max} = 100nm$.

c) Command moderation: The driving voltage u of the PEA is limited to $\pm 10V$, which contributes approximately an input v of $\pm 42\mu m$. Applying input signals beyond these values may destroy the actuator. In order to ensure that such overvoltage is avoided, a command moderation specification was also considered in controller synthesis. Thus, a reference input x_d within the $\pm 40\mu m$ operating range should generate a maximal operating driving command v of $\pm 40\mu m$, which ensures that the operating driving voltage u will be within $\pm 10V$.

3) Standard H_∞ problem and standard scheme: Three weighting functions $W_1(s)$, $W_2(s)$ and $W_3(s)$ were introduced (see Fig. 9-b) in order to fulfil the above specifications. In the figure, the reference x_d and the new disturbance Ω_w were considered as the exogenous inputs for the control synthesis, while the outputs to be controlled were the weighted outputs o_1 and o_2. Fig. 9-c represents augmented system P_{aug} that can be constructed on the basis of Fig. 9-b which incorporates the system $G(s)$ and the weightings $W_1(s)$, $W_2(s)$ and $W_3(s)$. According to the standard H_∞ problem, an optimal value $\gamma > 0$ and a controller $C(s)$ that stabilizes the standard scheme have to be determined in order to guarantee that [13]:

$$\|F_l\left(P_{aug}, C\right)\|_\infty < \gamma \tag{9}$$

where $F_l\left(P_{aug}, C\right)$ represents the lower linear fractional transformation (LFT) between $P_{aug}(s)$ and $C(s)$ which can be defined by:

$$\begin{pmatrix} o_1 \\ o_2 \end{pmatrix} = F_l\left(P_{aug}, C\right) \begin{pmatrix} x_d \\ \Omega_w \end{pmatrix}. \tag{10}$$

From Fig. 9-b, we have

$$\begin{cases} o_1 = W_1 S x_d - W_1 S W_3 \Omega_w \\ o_2 = W_2 C S x_d - W_2 C S W_3 \Omega_w, \end{cases} \tag{11}$$

where S is the sensitivity function $S = \frac{1}{(1+CG)}$. Using (10) and (11), the LFT can be expressed as:

$$F_l\left(P_{aug}, C\right) = \begin{pmatrix} W_1 S & -W_1 S W_3 \\ W_2 C S & -W_2 C S W_3 \end{pmatrix}. \tag{12}$$

According to condition (9) and the LFT in (12), the H_∞ problem becomes in finding an optimal value $\gamma > 0$ and a controller $C(s)$ such that

$$\begin{array}{ll} \|W_1 S\|_\infty < \gamma; & \|-W_1 S W_3\|_{<\infty} < \gamma; \\ \|W_2 C S\|_\infty < \gamma; & \|-W_2 C S W_3\|_\infty < \gamma \end{array} \tag{13}$$

which are similar if

$$\begin{array}{ll} |S| < \frac{\gamma}{|W_1|}; & |S| < \frac{\gamma}{|W_1 W_3|}; \\ |CS| < \frac{\gamma}{|W_2|}; & |CS| < \frac{\gamma}{|W_2 W_3|}; \end{array} \tag{14}$$

where $\frac{1}{W_1}$, $\frac{1}{W_1W_3}$, $\frac{1}{W_2}$ and $\frac{1}{W_2W_3}$ are called transfer functions (gabarits).

4) Derivation of the weighting functions: The weighting functions were calculated according to the specifications defined in Section. III-E.2. For the tracking performance specifications, we select:

$$\frac{1}{W_1} = \frac{s+1}{s+1000} \quad \Rightarrow \quad W_1 = \frac{s+1000}{s+1} \tag{15}$$

while for the command moderation, the maximal gain was chosen as:

$$\frac{1}{W_1W_2} = \frac{v^{\max}}{x_d^{\max}} = \frac{40\mu m}{40\mu m} = 1 \tag{16}$$

we can deduce that the weighting W_2:

$$W_2 = \frac{s+1}{s+1000} \tag{17}$$

For the disturbance rejection, the following gain was obtained from the worst case:

$$\frac{1}{W_1W_3} = \frac{e^{\max}}{\Omega_w^{\max}} = \frac{0.1\mu m}{3.825\mu m} = 0.026 \tag{18}$$

Consequently, the weighting W_3:

$$W_3 = 0.026\frac{s+1}{s+1000} \tag{19}$$

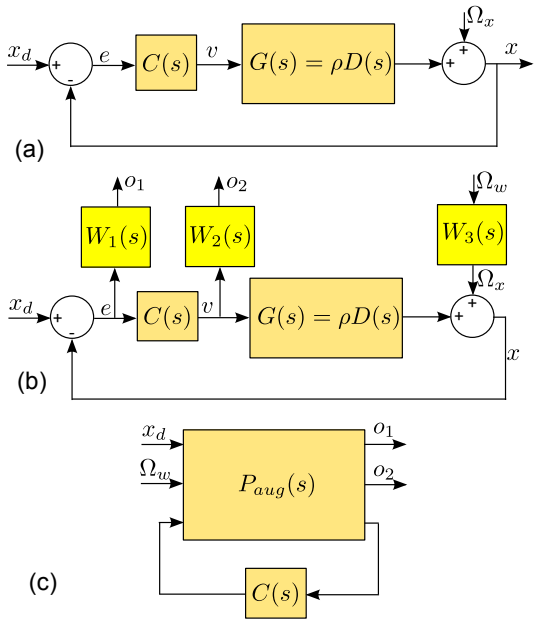

Fig. 9. (a) block diagram of the closed-loop, (b) block diagram of the closed loop augmented with the weightings, and (c)standard scheme.

5) Controller calculation: The controller $C(s)$ was calculated through the Doyle-Glover algorithm [14][15] to problem (14). The calculations revealed a controller of 11 order. This order was reduced to 5 without affecting the performances of the closed-loop system. The reduced controller which was calculated using the balanced realization/reduction technique [16] and the optimal value of γ were calculated as:

$$\begin{cases} C(s) = \frac{0.016\left(s+7.9\times10^6\right)\left(s^2+971s+4.6\times10^5\right)\left(s^2+43s+1.4\times10^7\right)}{(s+8.8\times10^4)(s+974)(s+1)(s^2+1153s+1.6\times10^7)} \\ \gamma = 1.69 \end{cases} \tag{20}$$

IV. Experimental results

The feedback controller $C(s)$ was employed to control the PEA in conjunction with the inverse compensator $\hat{\mathcal{P}}^{-1}$. Three different experiments were performed in order to explore the effectiveness of proposed methodology. In the first experiment a series of step reference x_d was applied to the closed-loop system in order to verify that the response of the system will not experience instability after a long period of time. The results under this input are depicted in Fig. 10-a. As the figure illustrates the stability is maintained as long as the constant input is beyond $1.5s$, which is sufficient relative to the response time of the PEA. A zoomed version of the step response Fig. 10-b shows that the settling time is (less than $2ms$), the overshoot is (0%) and the statical error is negligible which satisfy the tracking performance.

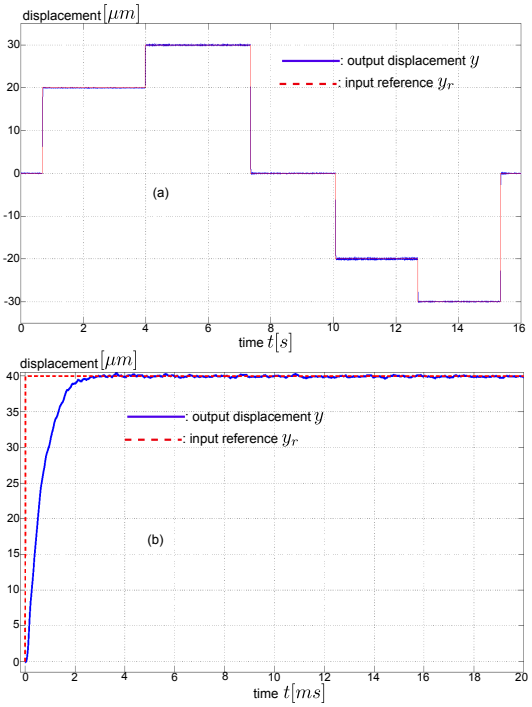

Fig. 10. Feedforward-feedback control of the PEA: (a) responses to a series of steps, and (b) a step response.

The next experiment was carried out by applying a sinusoidal reference input x_d under different excitations of frequency. The results are shown in Fig. 11, which illustrates that the tracking of a variable reference is well ensured by the controller even at frequency excitations larger than ($f = 0.1Hz$, see Fig. 4) which was considered for hysteresis identification.

The last experimental test was conducted by applying a sinusoidal input at different excitations of frequency within the $0.01Hz$ - $1kHz$ range such that the harmonic response of the closed-loop can be characterized. The results are summarized in Fig. 12 and compared to harmonic response of the PEA without the feedback-controller. As the figure illustrates the peak of resonance of the PEA was approximately at $400Hz$ without the controller, this peak which is completely removed with the synthesized closed-loop controller. In addition, the hysteresis of the PEA which represents the decay of the magnitude at low frequency was also cancelled out.

These experimental results demonstrate that the calculated H_∞ feedback controller can be employed to improve the tracking performance of the actuator with the feedforward inverse compensator.

V. Conclusions

A the formula that defines the output of the inverse compensation in conjunction with a feedback controller were employed to enhance the tracking performance of a plant. The experimental tests on a piezoelectric actuator revealed that this formula can be employed to synthesis an H_∞ feedback controller. These tests further clarified that the synthesized controller allowed tracking step as well as sinusoidal reference input at different excitations of frequency.

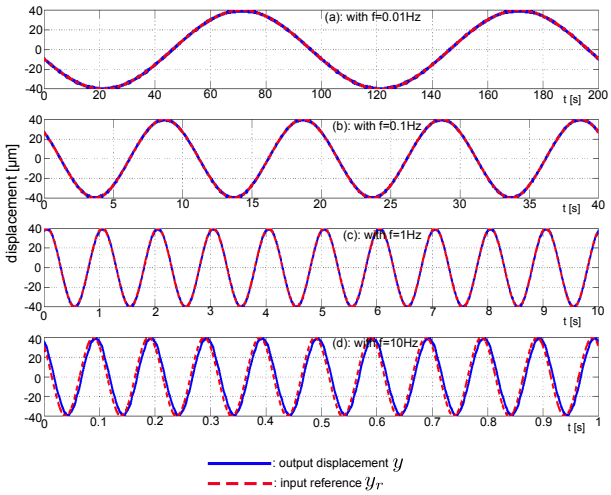

Fig. 11. Sinusoidal input reference tracking at different frequencies.

Acknowledgment

This work is supported by the French ANR-JCJC C-MUMS-project (National young investigator project ANR-12-JS03007.01: Control of Multivariable Piezoelectric Microsystems with Minimization of Sensors).

References

[1] M. Al Janaideh, "About the output of the inverse compensation of the Prandtl-Ishlinskii model," *Proceedings of the American Control Conference,* Washington, DC, pp. 247-252, 2013.

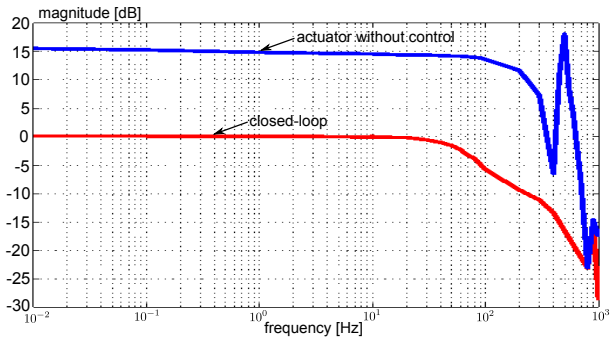

Fig. 12. Magnitude of the closed-loop compared with the magnitude of the actuator without control.

[2] M. Rakotondrabe, C. Clevy, and P. Lutz, "Complete open loop control of hysteretic, creeped, and oscillating piezoelectric cantilevers," *IEEE Transactions on Automation Science and Engineering*, vol. 7, no. 3, pp. 440-450, 2010.

[3] M. Rakotondrabe, "Bouc-Wen modeling and inverse multiplicative structure to compensate hysteresis nonlinearity in piezoelectric actuators," *IEEE Transactions on Automation Science and Engineering*, vol. 8, no. 2, pp. 428-431, 2011.

[4] Y. Feng, C. Rabbath, H. Hong, M. Al Janaideh, and C-Y. Su, "Robust control for shape memory alloy micro-actuators based flap positioning system," *Proceedings of the American Control Conference*, Baltimore, MD, pp. 4181-4186, 2010.

[5] R. Gorbet, K. Morris, and D. Wang, "Passivity-based stability and control of hysteresis in smart actuators," *IEEE Transactions on Control Systems Technologey*, vol. 9, no. 1, pp. 5-16, 2001, 2001.

[6] B. Jayawardhana, H. Logemann, and E. Ryan, "PID control of second-order systems with hysteresis," *International Journal of Control*, vol. 8, no. 8, pp. 13-31, 2008.

[7] L. Riccardi, D. Naso, B. Turchiano, and H. Janocha, "Design of linear feedback controllers for dynamic systems with hysteresis," *IEEE Transactions on Control Systems Technologey*, vol. 22, no. 4, pp. 1268 - 1280, 2014.

[8] J. Agnus, N. Chaillet, C. Clévy, S. Dembélé, M. Gauthier, Y. Haddab, G. Laurent, P. Lutz, N. Piat, K. Rabenorosoa, M. Rakotondrabe, and B. Tamadazte, "Robotic microassembly and micromanipulation at FEMTO-ST," *Journal of Micro-Bio Robotics*, vol. 8, no. 2, pp. 91-106, 2013.

[9] R. Wood, J. Whitney, and B. Finio, "Mechanics and Actuation for Flapping- Wing Robotic Insects," Published Editors: R. Blockley and W. Collection ,*Encyclopedia of Aerospace Engineering*, pp. 4393-4406, 2011.

[10] G. Bining, C. F. Quate, and Ch. Berger, "Atomic Force Microscope," *APS Physical Review Letters*, vol. 56, no. 9, pp. 930-933, 1986.

[11] Y. Zhu, W. Liu, K. Jia, W. Liao, and H. Xie, "A piezoelectric unimorph actuator based tip-tilt-piston micromirror with high fill factor and small tilt and lateral shift,", *Sensors and Actuators A: Physical*, 167, no. 2, pp. 495-501, 2011.

[12] L. Ljung, *System identification toolbox*, The Matlab user's guide, 1988.

[13] G. J. Balas, J. C. Doyle, K. Glover, A. Packard, and R. Smith, *μ-analysis and synthesis toolbox*, The Mathworks User's Guide-3, 2001.

[14] K. Glover and J. C. Doyle, "State-space formulae for all stabilizing controllers that satisfy an H_∞-norm bound and relations to risk sensivity," Systems & Control Letters, vol. 11, no. 3, pp.167-172, 1988.

[15] J. C. Doyle, K. Glover, P. K. Khargonekar and B. A. Francis, "State-space solutions to standard H_2 and H_∞ control problems," *IEEE Transactions on Automatic Control*, AC-34, no. 8, pp. 831-846, 1989.

[16] B. C. Moore, "Principal component analysis in linear systems: controllability, observability and model reduction," *IEEE Transaction on Automatic Control,* AC-26, no. 1, pp. 17-32, 1981.